NUCLEAR SCIENCE AND ENGINEERING: 122, 136–141 (1996)

Proton Emission in Reaction of 14.6-MeV Neutrons with Natural Iron

Bangjiao Ye, Yangmei Fan, Zhongmin Wang, and Rongdian Han

University of Science and Technology of China,
Department of Modern Physics, Hefei, Anhui 230026, China

and

Zhenxi Xiao

University of Science and Technology of China, Institute of Management, Beijing 100080, China

Received January 27, 1995
Accepted April 12, 1995

Abstract – *The energy spectra and angular distributions of proton emission in a reaction of $^{nat}Fe(n,xp)$ at a neutron energy of 14.6 MeV are measured by the University of Science and Technology of China multitelescope system. The double-differential cross sections of 16 reaction angles from 25 to 164.5 deg are obtained in this measurement. The statistical errors are reduced largely because of the thick target used. The angular distributions show a slightly energy-dependent forward-backward asymmetry. The angle-integrated proton spectrum is compared with theoretical calculations and other results. The total proton-emission cross section is in fair agreement with the prediction and evaluation.*

I. INTRODUCTION

The reaction of neutrons with structural materials to produce emitted charged particles is significant in the design of fission and fusion reactors. Bombarded by high fluxes of neutrons of ~14 MeV, structural materials must be very solid. The (n,xp) and $(n,x\alpha)$ reactions produce hydrogen and helium, which can affect the structural strength of materials and produce residual radioactivity. Knowing the strength, radioactivity, and lifetime of structural materials is of great economic importance.

Two techniques are generally used to measure neutron-induced charged-particle-emitted reaction cross sections: (a) the direct detection of emitted charged particles [with a time-of-flight (TOF) spectrometer, magnetic quadrupole spectrometers, and a multitelescope system] and (b) the detection of radiation emitted by the radioactive residual nuclei. Each has its advantages and limitations. The main shortcoming of radiochemical measurements is that they do not provide the energy and angular distribution cross-section information that can be measured in direct detection methods. But, there are two problems in the direct detection of emitted charged particles: low counting rates because of small producing cross sections and a thin target, and high backgrounds because of a large number of gamma-ray counts coming from the $(n,n'\gamma)$ and (n,γ) reactions and true background counts coming from the surroundings of the target.

Over the past 20 yr, some new detection systems have been developed to detect the emitted charged particles, for example, the charged-particle TOF spectrometer at Ohio University,[1] the magnetic quadrupole spectrometer at Lawrence Livermore National Laboratory,[2] and the multitelescope system at Vienna University[3] and the University of Science and Technology of China[4] (USTC). The energy and angular distributions of the emission of protons, deuterons, and alpha particles in neutron energy at <15-MeV ranges have been studied[5–8] with some structural materials. Iron is a very important structural material in nuclear engineering, so its data are very useful for the evaluation of radiation-induced material damage, radiation safety, neutron dosimetry, etc. With this aim in mind, double-differential proton emission cross sections have been

measured at USTC using the multitelescope system. Thick targets were used in this measurement, and the double-differential cross sections (DDCS) were derived by unfolding the thick-target spectra. In this way, the high-energy parts of the spectra could be measured with much better accuracy in same time as with the thin-target method, and also, the results are much less sensitive to the background.

II. EXPERIMENTAL PROCEDURE

Neutrons of 14.6 MeV were produced by the 150-kV Cockcroft-Walton accelerator at USTC. The multitelescope system, which is described in great detail in Ref. 4, is similar to the Vienna system. Here, we give only a brief explanation of this experiment.

A natural iron target is thick compared with the range of the most energetic (~15-MeV) protons. A metallic iron sheet 0.5 mm thick and 40 mm high was used. The whole chamber consisted of 32 telescopes. Sixteen telescopes were used for the measurement of the iron target, which was fixed in ring-shaped graphite, and the other 16 chambers were used for the simultaneous measurement of the background. Graphite was used for the target holder and the background-measured material because it has a very large negative Q value (−12.7 MeV) and very small cross sections of the (n,p) reaction. The proportional counters were operated with a gas mixture of 5% CO_2 and 95% argon at a gas pressure of 100 mb at a voltage of −750 V.

A 1-mm-high and 1-in.-diam CsI(Tl) crystal was used as the energy detector. The shielding material was 20 cm of iron to shield the CsI(Tl) from the neutrons. The distance between the neutron source (tritium-titanium target) and the CsI(Tl) was 400 mm. Monte Carlo methods (10^6 events) were used for the calculation of the reaction angular distribution function according to their geometric relation. The aperture function $W(\theta)$ of the 16 telescopes is shown in Fig. 1.

The whole system was irradiated for ~30 h at a neutron source strength of $\sim 1.5 \times 10^9$ n/s. During the entire experiment, one background telescope was equipped with a weak ^{241}Am alpha-particle source, and another was equipped with polyethylene foil. These telescopes were used to monitor the energy calibration of the CsI(Tl) crystal. The stability of the entire measuring system was checked continually by monitoring all of the important single counter rates. The target foil was rotated 180 deg at the midpoint of the experiment to reduce the asymmetry effects due to the two different halves of the reaction chamber. The total number of true events turned out to be ~170 000.

III. DATA ANALYSIS AND RESULTS

By selecting the appropriate channel range of the particle pulse-shape spectra and the flight-time spectra,

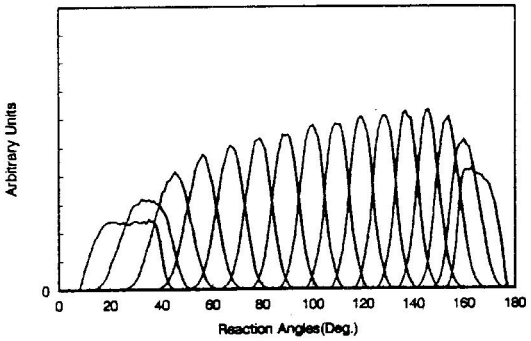

Fig. 1. The angular acceptance functions of the various telescopes.

the chance coincidence counts, alpha particles, and gamma rays were eliminated. The true background was eliminated by the subtraction of the background energy spectra from the corresponding foreground energy spectra, channel by channel. In this way, thick-target proton energy spectra were obtained for 16 reaction angles from 25.0 to 164.5 deg, as shown in Fig. 2. The measured thick-target spectra $N(E_p)$ had to be unfolded to obtain the proton-emission spectra. This was done by numerically differentiating the quantity $(dE_p/dX)\cdot N(E_p)$ with respect to E_p. This progress was similar to that of Ref. 8. After this step, all thick-target spectra were transformed into equivalent thin-target spectra. These results are all in the laboratory

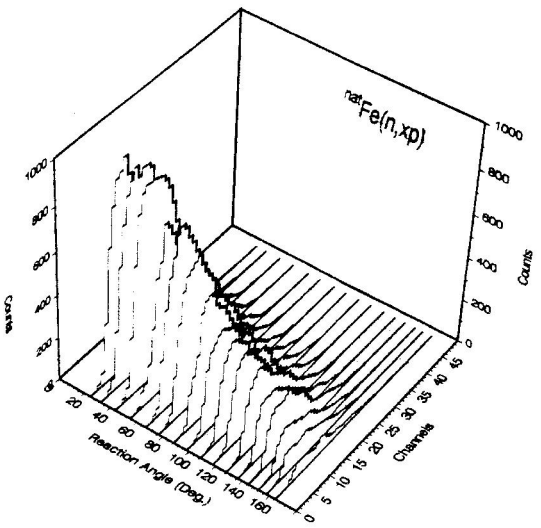

Fig. 2. Thick-target proton energy spectra obtained from this experiment for 16 reaction angles.

system. The conversion of these results in the center-of-mass (c.m.) system is made by using the nuclear reaction formula. However, the angle-integrated energy spectra in the c.m. system as well as the laboratory system should be similar because the target nuclei have large masses.

The double-differential proton emission cross sections were obtained for 16 reaction angles with an angular resolution of 12 deg on average. Both the experimental data and the errors are listed in Table I in the c.m. system. The errors in Table I consist of two parts of statistical errors and all identified systematic error contributions. The statistical error corresponding to 1σ of errors is small because of the large true events in this measurement. The total systematic error is 6.2%, which consists of a neutron flux error of 3.3%, a target height error of 2%, a solid angle of the central detector error of 3%, a dE/dx value error of 2%, a data reduction procedure error of 2%, and other possible uncertainties of 3%.

Because of high background counts in low-energy parts, the DDCS of proton emission has not been measured up to 3 MeV. The proton energy of 3 to 4 MeV can be measured only for five angles of 43.9, 77.1, 136.6, 157.8, and 164.5 deg.

The angle-integrated proton-emission cross sections were derived from least-squares fits of Legendre polynomials up to $l = 2$ to the $(d^2\sigma/dE_p d\theta)$ values. The results of this calculation are listed in Table II. The total proton-emission cross section for proton energy for >3-MeV regions is 170.7 ± 13.7 mb.

IV. COMPARISON AND DISCUSSION

The angular distributions of the proton emission from this measurement are shown in Fig. 3 in 2-MeV bins. The solid lines in Fig. 3 are the predictions of the systematics of Kalbach and Mann[9] where the values of $a_0^{MSD}(\epsilon_p)/[a_0^{MSD}(\epsilon_p) + a_0^{MSC}(\epsilon_p)]$ are 0.4, 0.6, and 0.8 for $\epsilon_p = 6$ to 8, 8 to 10, and 10 to 12 MeV, the differential cross sections $a_0^{MSD}(\epsilon_p)$ and $a_0^{MSC}(\epsilon_p)$ for the multistep statistical direct (MSD) and multistep statistical compound (MSC) processes. Figure 3 shows that

TABLE I

DDCS of the ^{nat}Fe(n,xp) Reaction at $E_n = 14.6$ MeV

E_p (MeV)	Reaction Angles (deg)							
	25.0	32.8	43.9	55.0	67.2	77.1	88.3	98.3
3 to 4			3.33 ± 0.24			2.88 ± 0.20		
4 to 5	2.30 ± 0.19	3.18 ± 0.23	2.77 ± 0.15	2.77 ± 0.20	3.43 ± 0.27	3.03 ± 0.21	3.51 ± 0.29	3.06 ± 0.17
5 to 6	2.22 ± 0.18	2.88 ± 0.21	3.39 ± 0.29	2.02 ± 0.15	3.07 ± 0.24	3.17 ± 0.24	3.34 ± 0.22	3.34 ± 0.28
6 to 7	3.63 ± 0.24	3.02 ± 0.21	2.50 ± 0.17	1.82 ± 0.13	1.57 ± 0.12	1.98 ± 0.14	2.22 ± 0.15	2.78 ± 0.19
7 to 8	2.52 ± 0.17	1.89 ± 0.13	1.91 ± 0.13	1.60 ± 0.11	1.99 ± 0.13	1.93 ± 0.13	1.82 ± 0.13	1.43 ± 0.11
8 to 9	1.29 ± 0.09	1.14 ± 0.08	0.68 ± 0.06	1.18 ± 0.08	0.95 ± 0.07	0.96 ± 0.07	1.12 ± 0.08	0.62 ± 0.06
9 to 10	0.94 ± 0.07	0.66 ± 0.05	1.03 ± 0.07	0.50 ± 0.04	0.73 ± 0.05	0.54 ± 0.05	0.38 ± 0.04	0.66 ± 0.06
10 to 11	0.30 ± 0.03	0.36 ± 0.03	0.25 ± 0.03	0.36 ± 0.03	0.54 ± 0.04	0.33 ± 0.03	0.49 ± 0.04	0.32 ± 0.03
11 to 12	0.12 ± 0.02	0.05 ± 0.02	0.25 ± 0.02	0.28 ± 0.02	0.05 ± 0.01	0.08 ± 0.02	0.06 ± 0.01	0.01 ± 0.02
12 to 13	0.02 ± 0.01	0.06 ± 0.01	0.01 ± 0.01	0.04 ± 0.01	0.08 ± 0.01	0.11 ± 0.01	0.02 ± 0.01	0.13 ± 0.01
13 to 14	0.05 ± 0.01	0.01 ± 0.00	0.03 ± 0.00	0.06 ± 0.01	0.01 ± 0.00	0.02 ± 0.01	0.00 ± 0.00	0.02 ± 0.01

E_p (MeV)	Reaction Angles (deg)							
	108.6	117.9	128.0	136.6	144.3	151.9	157.8	164.5
3 to 4				2.04 ± 0.16			1.94 ± 0.15	1.42 ± 0.16
4 to 5	3.62 ± 0.30	3.73 ± 0.31	3.50 ± 0.26	3.07 ± 0.21	1.03 ± 0.11	1.35 ± 0.12	0.21 ± 0.08	1.10 ± 0.11
5 to 6	3.34 ± 0.27	2.77 ± 0.19	2.99 ± 0.20	3.36 ± 0.22	2.04 ± 0.15	0.95 ± 0.10	0.90 ± 0.10	0.46 ± 0.09
6 to 7	2.62 ± 0.18	2.10 ± 0.15	1.55 ± 0.12	1.04 ± 0.09	2.33 ± 0.16	1.88 ± 0.13	0.87 ± 0.08	0.59 ± 0.08
7 to 8	1.80 ± 0.13	1.75 ± 0.12	1.54 ± 0.11	1.62 ± 0.11	1.02 ± 0.08	0.88 ± 0.08	0.93 ± 0.08	0.33 ± 0.06
8 to 9	1.02 ± 0.08	1.03 ± 0.08	1.20 ± 0.09	0.85 ± 0.07	0.49 ± 0.05	0.44 ± 0.05	0.36 ± 0.05	0.10 ± 0.05
9 to 10	0.60 ± 0.05	0.60 ± 0.05	0.77 ± 0.06	0.46 ± 0.04	0.40 ± 0.04	0.34 ± 0.04	0.33 ± 0.04	0.66 ± 0.06
10 to 11	0.23 ± 0.03	0.27 ± 0.03	0.07 ± 0.02	0.35 ± 0.03	0.19 ± 0.02	0.17 ± 0.02	0.06 ± 0.02	0.02 ± 0.03
11 to 12	0.26 ± 0.02	0.16 ± 0.02	0.18 ± 0.02	0.09 ± 0.02	0.16 ± 0.02	0.02 ± 0.01	0.04 ± 0.01	0.05 ± 0.02
12 to 13	0.03 ± 0.01	0.01 ± 0.01	0.12 ± 0.01	0.01 ± 0.01	0.03 ± 0.01	0.03 ± 0.01	0.04 ± 0.01	0.08 ± 0.02
13 to 14	0.00 ± 0.00	0.04 ± 0.00	0.01 ± 0.00	0.01 ± 0.00	0.04 ± 0.00	0.04 ± 0.01	0.03 ± 0.01	0.02 ± 0.01

TABLE II

The Angle-Integrated Proton-Emission Cross Section from the ^{nat}Fe(n,xp) Reaction

E_p (MeV)	$d\sigma/d\epsilon$ (mb/MeV)
3 to 4	33.78 ± 3.28
4 to 5	34.31 ± 4.88
5 to 6	33.89 ± 4.23
6 to 7	24.32 ± 3.90
7 to 8	20.81 ± 2.06
8 to 9	10.92 ± 1.56
9 to 10	7.18 ± 0.97
10 to 11	3.63 ± 0.59
11 to 12	1.20 ± 0.48
12 to 13	0.46 ± 0.20
13 to 14	0.16 ± 0.07

the angular distribution of the proton emission from the natural iron (n,xp) reaction is not as strong as that of the Kalbach-Mann predictions. Similar behavior has been found in the proton spectrum from a natural nickel (n,xp) reaction, which we are just measuring. These discrepancies need further theoretical and experimental analyses.

In 1979, the Grimes group obtained measurement results for ^{54}Fe, ^{56}Fe, and natural iron (n,xp) reactions at $E_n = 14.8$ MeV. The Grimes data have been extensively used to test the nuclear reaction models. A comparison of the current results of the angle-integrated cross sections with the Grimes results is given in Fig. 4. In the highest energy region, our values are slightly smaller than those of the Grimes data, but our values agree with the Grimes data within the errors.

The theoretical calculation was given by Zhang,[10] of the Chinese Nuclear Data Center (CNDC), who used the UNF code, which is developed for the calculations of fast neutron data for structural materials. For structural materials at incident neutron energies below 20 MeV, it is demonstrated that the constructed model contains the Hauser-Feshbach, Weisskopf-Ewing as well as the exciton models as limiting cases. The unified treatment of pre-equilibrium processes includes a number of interesting features such as the exciton state densities with the exact Pauli exclusion correction, which are renormalized to the backshifted Fermi-gas formula, and the introduction of formation factors of composite particles in calculations of the pickup-type composite particle emission. The result of the calculation was obtained for only $n + {}^{56}$Fe at $E_n = 14.5$ MeV. Because ^{56}Fe has a >90% abundance in natural iron, similar energy spectra for natural iron and ^{56}Fe would be expected. In Fig. 5, the calculated result of ^{56}Fe is compared with the experimental data of natural iron. The calculated spectrum ends a little below 12 MeV while the measured spectrum extends above 14 MeV because of different reaction thresholds for ^{56}Fe(n,p) and ^{54}Fe(n,p). At CNDC, a UNF2 code is being developed for the calculation of the energy spectrum of

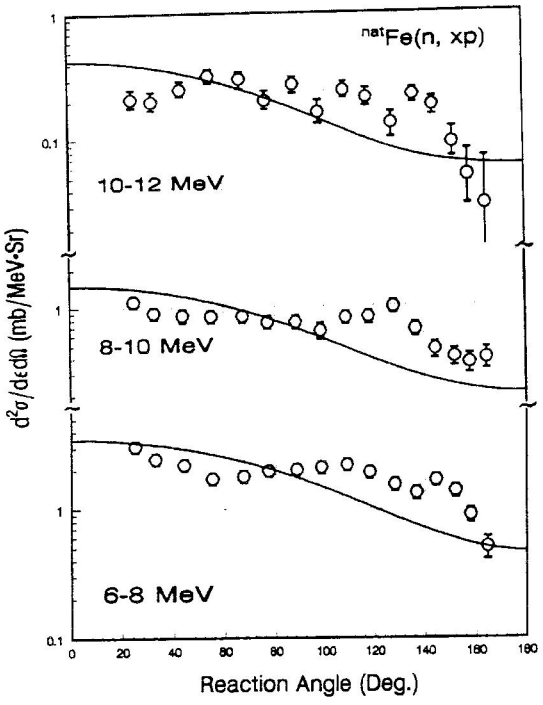

Fig. 3. The angular distributions of the proton emission from the ^{nat}Fe(n,xp) reaction in 2-MeV energy regions.

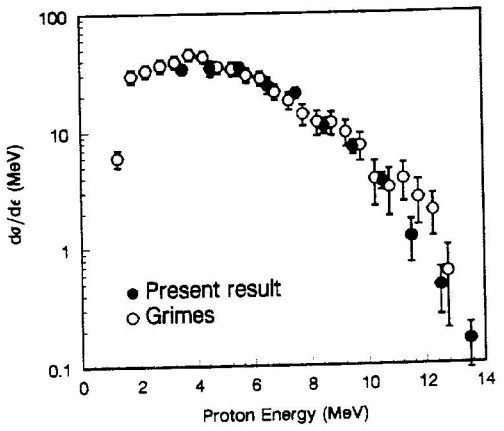

Fig. 4. Proton spectra from the ^{nat}Fe(n,xp) reaction.

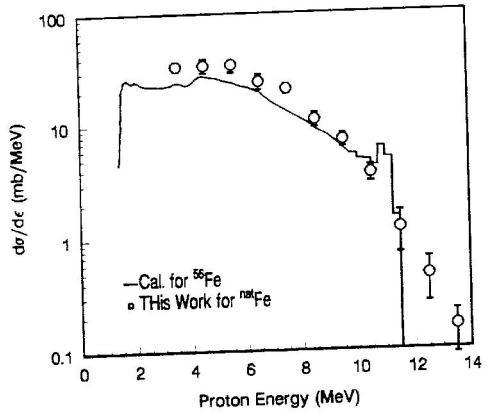

Fig. 5. Comparison of this result with the calculated result.

natural material. When this code is completed, a detailed comparison of this result with the theoretical calculation for natural iron will be given.

The evaluations of total (angle-energy-integrated) proton-emission cross sections have been carried out by CNDC, BROND, ENDF/B-VI, and JENDL-3 for iron.[11] These results and the Grimes data are shown in Table III. The evaluation of proton emission from natural iron in Table IV is obtained from Table III with all the isotope cross sections according to their abundance added. The experimental results of Grimes[12] and the current research are also listed in Table IV. For the $E_p > 3$ MeV portions, the current result is lower by 6% than that of the Grimes data.

ACKNOWLEDGMENTS

The authors would like to thank the personnel of CNDC for their support and D. L. Zhou, Q. C. Lian, and Q. B. Shen for their kind help and suggestions. This work was supported in part by the General Company of Nuclear Industry of China and the Young Funds of USTC.

REFERENCES

1. S. K. SARAF, C. E. BRIENT, P. M. EGUN, S. M. GRIMES, V. MISHRA, and R. S. PEDRONI, "Cross Sections and Spectra for the ^{54}Fe and ^{56}Fe(n,xp) and $(n,x\alpha)$ Reactions Between 8 and 15 MeV," *Nucl. Sci. Eng.*, **107**, 365 (1991).

TABLE III

Proton-Emission Cross Sections of Iron (mb)

Isotopes and Their Abundance in Natural Iron		Evaluation				Measurement
		E_n = 14.1 MeV				E_n = 14.8 MeV Grimes
		CNDC	BROND	B-VI	JENDL-2	
5.9%	^{54}Fe	766	618	868	854	900 ± 110
91.72%	^{56}Fe	155	166	165	173	190 ± 22
2.1%	^{57}Fe	71		68		
0.28%	^{58}Fe	133		11		

TABLE IV

Proton-Emission Cross Sections of Natural Iron (mb)

E_p (MeV)	Evaluation				Measurement	
	E_n = 14.1 MeV				E_n = 14.8 MeV Grimes	E_n = 14.6 MeV Current Research
	CNDC	BROND	B-VI	JENDL-3		
1 to 14	189	191[a]	204	222	230 ± 30	171 ± 14
3 to 14					181 ± 24	

[a]Because there is no evaluation data for ^{57}Fe and ^{58}Fe, the CNDC data were used.

2. S. M. GRIMES, R. C. HAIGHT, K. R. ALVAR, H. H. BARSCHALL, and R. R. BORCHERS, *Phys. Rev. C*, **19**, 2127 (1979); see also S. M. GRIMES and R. C. HAIGHT, and J. D. ANDERSON, *Phys. Rev. C*, **17**, 508 (1978).

3. G. TRAXLER, R. FISCHER, and H. VONACH, "A Multiwire Proportional Chamber for the Measurement of Differential (n, Charged Particle) Cross-Sections," *Nucl. Instrum. Methods*, **217**, 121 (1983).

4. B. J. YE, Y. M. FAN, Z. M. WANG, R. D. HAN, W. MEI, X. Q. YU, Y. M. YANG, R. Y. HAN, H. J. DU, and Z. X. XIAO, "Development of a Multitelescope System for Measurement of Differential (n, Charged Particle) Reaction," *Commun. Nucl. Data Prog.*, **10**, 19 (1993).

5. S. L. GRAHAM, M. AHMAD, S. M. GRIMES, H. SATYANARAYANA, and S. K. SARAF, "Cross Sections and Spectra for (n,xp) and $(n,x\alpha)$ Reactions on ^{58}Si and ^{60}Ni at Energies of 9.4 and 11 MeV," *Nucl. Sci. Eng.*, **95**, 60 (1987).

6. M. AHMAD, S. L. GRAHAM, S. M. GRIMES, H. SATYANARAYANA, S. K. SARAF, and S. STRICKLIN, "Total Charged-Particle Emission Cross Sections for 9.4- and 11-MeV Neutron Bombardment of Type 316 Stainless Steel," *Nucl. Sci. Eng.*, **90**, 311 (1985).

7. G. TRAXLER, A. CHALUPKA, R. FISCHER, B. STROHMAIER, M. UHL, and H. VONACH, "Investigation of the ^{93}Nb(n,xp) Reaction at $E_n = 14.1$ MeV," *Nucl. Sci. Eng.*, **90**, 174 (1985); see also R. FISCHER, M. UHL, and H. VONACH, "^{93}Nb(n,xp), ^{nat}Ag(n,xp), and ^{nat}In(n,xp) Reaction at 14.1 MeV," *Phys. Rev. C*, **37**, 58 (1988).

8. B. J. YE, Y. M. FAN, Z. M. WANG, R. D. HAN, and Z. X. XIAO, "The ^{93}Nb(n,xp) Reaction at $E_n = 14.6$ MeV," *Nucl. Sci. Eng.*, **117**, 67 (1994).

9. C. KALBACH and F. M. MANN, "Phenomenology of Continuum Angular Distributions I. Systematics and Parameterization," *Phys. Rev. C*, **23**, 112 (1981); see also C. KALBACH, "Possible Energy Parameters for Continuum Angular Distributions," *Phys. Rev. C*, **25**, 3197 (1982).

10. J. S. ZHANG, "A Unified Hauser-Feshbach and Exciton Model for Calculating Double-Differential Cross Sections of Neutron-Induced Reactions Below 20 MeV," *Nucl. Sci. Eng.*, **114**, 55 (1993).

11. D. L. ZHOU, J. ZHANG, and T. LIU, Final Report for IAEA Contract Nr. 5962/R1/RB.

12. Q. C. LIAN, "Nuclear Data Library," Chinese Nuclear Data Center.